The condensin complex is a mechanochemical motor that translocates along DNA

Tsuyoshi Terakawa[1,*], Shveta Bisht[2,*], Jorine M. Eeftens[3,*],

Cees Dekker[3,†], Christian H. Haering[2,†], and Eric C. Greene[1,†]

[1]Department of Biochemistry and Molecular Biophysics, Columbia University, New York, NY, USA

[2]Cell Biology and Biophysics Unit, Structural and Computational Unit, European Molecular Biology Laboratory (EMBL), Heidelberg, Germany

[3]Department of Bionanoscience, Kavli Institute of Nanoscience Delft, Delft University of Technology, Delft, Netherlands

[†]Corresponding authors: c.dekker@tudelft.nl (C.D.); christian.haering@embl.de (C.H.H.); ecg2108@cumc.columbia.edu (E.C.G.).

[*]These authors contributed equally to this work.

Condensin plays crucial roles in chromosome organization and compaction, but the mechanistic basis for its functions remains obscure. We used single-molecule imaging to demonstrate that *Saccharomyces cerevisiae* condensin is a molecular motor capable of adenosine triphosphate hydrolysis–dependent translocation along double-stranded DNA. Condensin's translocation activity is rapid and highly processive, with individual complexes traveling an average distance of ≥10 kilobases at a velocity of ~60 base pairs per second. Our results suggest that condensin may take steps comparable in length to its ~50-nanometer coiled-coil subunits, indicative of a translocation mechanism that is distinct from any reported for a DNA motor protein. The finding that condensin is a mechanochemical motor has important implications for understanding the mechanisms of chromosome organization and condensation.

Structural maintenance of chromosomes (SMC) complexes are the major organizers of chromosomes in all living organisms (1, 2). These protein complexes play essential roles in sister chromatid cohesion, chromosome condensation and segregation, DNA replication, DNA damage repair, and gene expression. A distinguishing feature of SMC complexes is their large ring-like configuration, the circumference of which is made up of two SMC coiled-coil subunits and a single kleisin subunit (Fig. 1A) (1–4). The ~50-nm-long antiparallel coiled-coil subunits are connected at one end by a stable dimerization interface, referred to as the hinge domain, and at the other end by globular adenosine triphosphatase (ATPase) domains belonging to the ATP-binding cassette family (5). The ATPase domains are bound by a protein of the kleisin family, along with additional accessory subunits, which vary for different types of SMC complexes (Fig. 1A). The relationship between SMC structures and their functions in chromosome organization is not completely understood
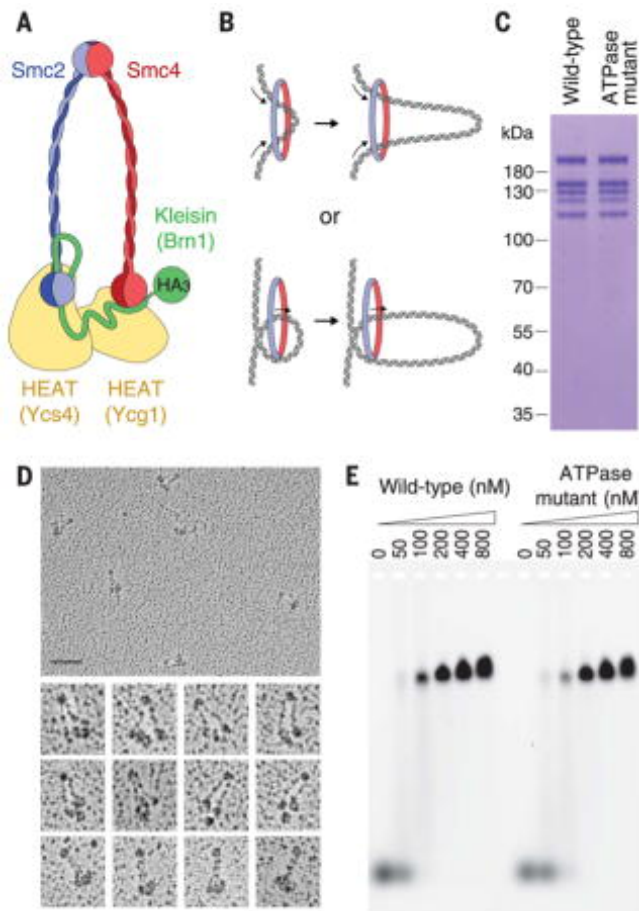
Fig. 1 | Biochemistry of budding yeast condensin holocomplexes. (A) Schematic of the *S. cerevisiae* condensin complex. The Brn1 kleisin subunit connects the ATPase head domains of the Smc2-Smc4 heterodimer and recruits the HEAT-repeat subunits Ycs4 and Ycg1. The cartoon highlights the position of the HA$_3$ tag used for labeling. **(B)** Conceptual schematic of loop extrusion for models with either two (top) or one (bottom) DNA strand(s) passing through the center of the SMC ring. **(C)** Wild-type and ATPase-deficient Smc2(Q147L)-Smc4(Q302L) condensin complexes analyzed by SDS–polyacrylamide gel electrophoresis and Coomassie staining (Q, glutamine; L, leucine). **(D)** Electron micrographs of wild-type condensin holocomplexes rotary-shadowed with platinum/carbon. Scale bars, 100 nm. **(E)** Electrophoretic mobility shift assays with a 6-carboxyfluorescein–labeled 45-bp dsDNA substrate (100 nM) and the indicated protein concentrations. **(F)** ATP hydrolysis by wild-type and ATPase mutant condensin complexes (0.5 μM) upon addition of increasing concentrations of a 6.4-kb linear DNA at saturated ATP concentrations (5 mM). The plot shows means ± SD from three (wild-type) or two (ATPase mutant) independent experiments. **(G)** Michaelis-Menten kinetics for the rate of ATP hydrolysis by wild-type condensin complexes (0.5 μM) at increasing ATP concentrations in the presence of 240 nM 6.4-kb linear DNA. The plot shows means ± SD from three independent experiments. The fit corresponds to a K_m of 0.4 ± 0.07 mM for ATP and a k_{cat} of 2.0 ± 0.1 s^{-1} per molecule of condensin (mean ± SE).

(6), but many models envision that the coiled-coil domains allow the complexes to topologically embrace DNA (1–4). Given the general resemblance to myosin and kinesin, some early models postulated that SMC proteins might be mechano-chemical motors (7–10). SMC complexes are thought to regulate genome architecture by physically linking distal chromosomal loci, but how these bridging interactions might be established is unknown (1, 2, 11). An early model suggested that many three-dimensional (3D) features of eukaryotic chromosomes might be explained by DNA loop extrusion (Fig. 1B) (12, 13), and recent polymer dynamics simulations have shown that loop extrusion can recapitulate the formation of topologically associating domains, chromatin compaction, and sister chromatid segregation (14–18). This loop extrusion model assumes a central role for SMC complexes in actively creating the DNA loops (11, 12). Similarly, it has been proposed that prokaryotic SMC proteins may structure bacterial chromosomes through an active loop extrusion mechanism (19–21). However, the loop extrusion model

remains hypothetical, in large part because the motor activity that is necessary for driving loop extrusion could not be identified (11). The absence of an identifiable motor activity in SMC complexes instead has lent support to alternative models in which DNA loops are not actively extruded but rather are captured and stabilized by stochastic pairwise SMC binding interactions to bridge distal loci (22).

To help distinguish between possible mechanisms of SMC protein–mediated chromosomal organization, we examined the DNA binding properties of condensin (23). We overexpressed the five subunits of the condensin complex in budding yeast and purified the complex to
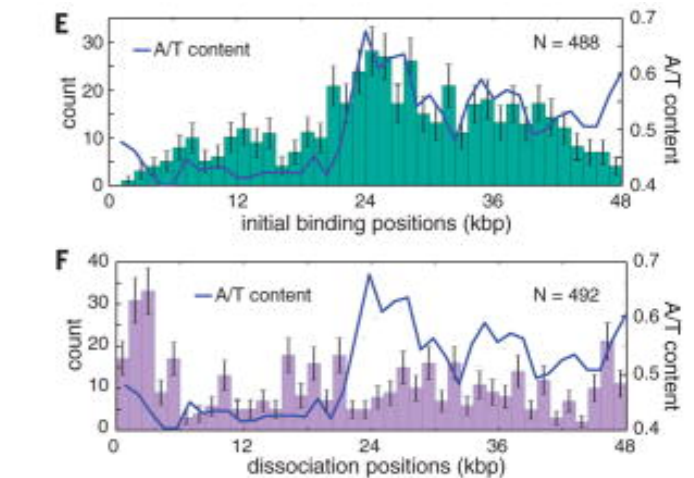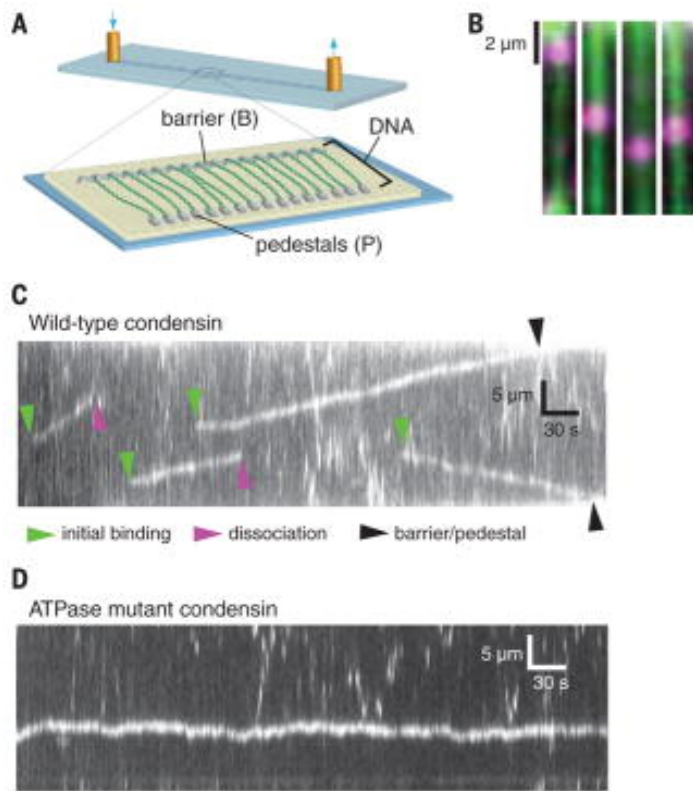
Fig. 2 | DNA curtain assay for DNA binding activity of condensin. (**A**) Schematic of the double-tethered DNA curtain assay (up and down arrows, inlet and outlet of buffer, respectively). (**B**) Still images showing Qdot-tagged condensin (magenta) bound to YoYo1-stained DNA (green). (**C**) Kymograph showing examples of Qdot-tagged condensin translocating on a single DNA molecule (unlabeled); the initial condensin binding sites, dissociation positions, and collisions with the barriers or pedestals are highlighted with color-coded arrowheads. (**D**) Kymograph showing Qdot-tagged ATPase-deficient mutant Smc2(Q147L)-Smc4(Q302L) condensin undergoing 1D diffusion on DNA (unlabeled). (**E**) Initial binding site and (**F**) dissociation site distributions of condensin superimposed on the A/T content of the λ-DNA substrate. All reactions contained 4 mM ATP. Error bars in (E) and (F) represent SD calculated by boot strap analysis. kbp, kilobase pairs.

homogeneity (Fig. 1C and fig. S1). Electron microscopy images confirmed that the complexes were monodisperse (Fig. 1D). As previously described for electron micrographs of immunopurified *Xenopus laevis* or human condensin (24), we observed electron density that presumably corresponds to the two HEAT-repeat subunits in close vicinity to the Smc2-Smc4 ATPase head domains. We confirmed that the *Saccharomyces cerevisiae* condensin holocomplex binds double-stranded DNA (dsDNA) and hydrolyzes ATP in vitro (Fig. 1, E and F). Addition of dsDNA stimulated the condensin ATPase activity so that it increased about threefold, which is consistent with previous measurements with *X. laevis* condensin I complexes (25). We found a Michaelis constant (Km) and catalytic rate constant (k_{cat}) of 0.4 ± 0.07 mM and 2.0 ± 0.1 s−1, respectively (means ± SE), for ATP hydrolysis in the presence of linear dsDNA (Fig. 1G). Furthermore, condensin promoted extensive ATP hydrolysis–dependent DNA compaction of single-tethered DNA curtains, which was reversible by increasing the salt concentration to 0.5 M NaCl (fig. S2, A to C). An ATPase-deficient version of condensin with mutations in the γ-

phosphate switch loops (Q-loops) of Smc2 and Smc4 still bound DNA (Fig. 1E) but exhibited no ATP hydrolysis activity (Fig. 1F) or DNA compaction activity (fig. S2D).

We then used total internal reflection fluorescence microscopy to visualize binding of single fluorescently tagged condensin holocomplexes to double-tethered DNA substrates (26). We fluorescently labeled condensin with quantum dots (Qdots) conjugated to antibodies against triple copies of the hemagglutinin (HA3) tag fused to the Brn1 kleisin subunit (Fig. 1A). Electrophoretic mobility shift assays confirmed that condensin was quantitatively labeled (fig. S3A). Importantly, binding to the Qdots inhibited neither condensin's ATP hydrolysis activity nor its ability to alter DNA topology (fig. S3, B and C). We prepared double-tethered curtains by attaching the DNA substrates (~48.5–kb λ-DNA) to a supported lipid bilayer through a biotin-streptavidin linkage; we then aligned one end of the DNA molecules at nanofabricated chromium

(Cr) barriers and anchored the other end to Cr pedestals located 12 μm downstream (Fig. 2A) (26).

Using double-tethered curtains, we were able to detect binding of condensin complexes to individual DNA molecules (Fig. 2B). Although we observed single Qdot-tagged condensin complexes, we do not yet know whether the observed complexes were single condensin molecules or condensin oligomers. Kymographs revealed that ~85% of all bound condensin complexes (n = 671) underwent linear motion along the DNA (Fig. 2C and movie S1). The up or down direction of movement was random, but once a complex started to translocate, it generally proceeded unidirectionally without a reversal of direction (reversals were observed occasionally, in 6% of the traces).

Condensin has not been previously shown to act as a molecular motor, but the observed movement is fully consistent with expectations for ATP-dependent translocation of a motor protein along DNA. Unlike the wild-type condensin, the ATPase-deficient Q-loop mutant of condensin only exhibited motion consistent with random 1D diffusion (Fig. 2D). Wild-type condensin in the presence of the nonhydrolyzable ATP analog ATPγS also displayed only 1D diffusion (fig. S4A). Previous single-molecule experiments demonstrated rapid 1D diffusion of cohesin on DNA but found no evidence for ATP-dependent translocation, suggesting that there may be differences in how the two SMC complexes process DNA (27, 28).

Analysis of the initial binding positions for wild-type condensin revealed a preferential binding to A/T-rich regions (Pearson's r = 0.66, P = 5 × 10−6; Fig. 2E), similar to that reported for *Schizosaccharomyces pombe* cohesin (27). In contrast, the condensin dissociation positions were not correlated with A/T content (Pearson's r = −0.05, P = 0.77), nor were there any other preferred regions for dissociation within the DNA, with the exception of the Cr barriers and pedestals (Fig. 2F). These findings are consistent with a model where condensin loads at A/T-rich sequences and then translocates away.
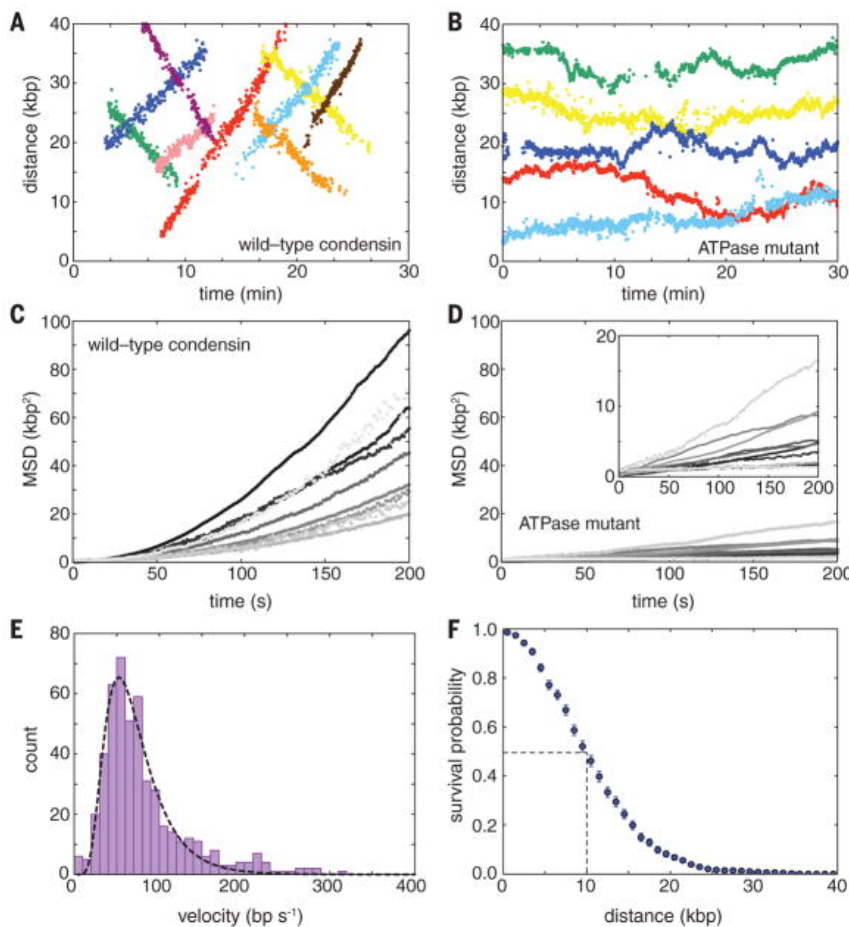
We used particle tracking to quantitatively analyze the movement of condensin on DNA (Fig. 3, A and B; fig. S4B; and data S1). Wild-type condensin did not travel in a preferred direction; rather, 52% (255/491) of the complexes went one direction, and 48% (236/491) went the opposite direction. The condensin ATPase mutant did not exhibit any evidence of unidirectional

Fig. 3 | Condensin is an ATP-dependent mechanochemical molecular motor. (**A**) Examples of tracked translocation trajectories for Qdot-tagged wild-type condensin and (**B**) for the ATPase-deficient Smc2(Q147L)-Smc4(Q302L) condensin mutant. (**C**) Mean squared displacement (MSD) plots for wild-type condensin and (**D**) for the ATPase-deficient mutant, obtained from the tracked trajectories. The inset in (D) is a magnification of the main curves. (**E**) Velocity distributions for condensin translocation activity. The dashed line is a log-normal fit to the translocation rate data. (**F**) Processivity measurements of condensin motor activity. The dashed line highlights the translocation distance corresponding to dissociation of one half of the bound condensin complexes. Error bars represent SD calculated by boot strap analysis.

translocation. Mean squared displacement (MSD) plots generated from condensin tracking data exhibited increasing slopes (Fig. 3C), which is only consistent with directed motion (29). In contrast, MSD plots were linear for the ATPase-deficient condensin mutant (Fig. 3D) and for wild-type condensin in the presence of ATPγS (fig. S4C). Linear MSD plots were characteristic of random diffusive motion (29), yielding diffusion coefficients of $(1.7 \pm 1.4) \times 10{-3}$ and $(0.8 \pm 1.0) \times 10{-3}$ μm2 s−1 (means ± SD) for ATPase-deficient condensin and wild-type condensin plus ATPγS, respectively.

We used the tracking data to determine the velocity and processivity of wild-type condensin. A plot of the velocity distributions for data collected in the presence of saturated concentrations of ATP (4 mM; Fig. 1G) was well described by a log-normal distribution, revealing a mean apparent translocation velocity of 63 ± 36 base pairs (bp) s−1 (16 ± 9 nm s−1; means ± SD; n = 491) (Fig. 3E). Upon initial binding, condensin paused for a brief period (τ_{pause} = 13.3 ± 1.5 s; mean ± SD) before beginning to move along the DNA, which suggests the existence of a rate-limiting step before condensin becomes active for translocation (Fig. 2C and fig. S5). Each translocating condensin complex remained bound to the DNA for an average total time of 4.7 ± 0.2 min and traveled an average of 10.3±0.4 kb (2.6 ± 0.1 μm; means ± SD) before dissociating (Fig. 3F and fig. S6A). These values provide merely a lower limit of the processivity of condensin, because a considerable fraction (42%) of the complexes traveled all the way to the ends of the 48.5-kb λ-DNA, where they collided with the Cr barriers or pedestals (for example, Fig. 2C). There was no correlation between translocation velocity and processivity at a given ATP concentration (Pearson's r = 0.035, P = 0.43 at 4 mM ATP) (fig. S6B). However, velocity and processivity both varied with ATP concentrations. From Michaelis-Menten analysis, we found a maximum velocity of 62 ± 2 bp s−1 and a Km of 0.2 ± 0.04 mM ATP (means ± SD) (fig. S7, A and B). The initial pause time (τ_{pause}) also varied with ATP concentration, from 3.9 ± 0.8 min at 50 μM ATP to 13.3 ± 1.5 s at 4 mM ATP (means ± SD), suggesting that this delay reflects a transition from a translocation-inactive to a translocation-active state that is dependent on ATP binding, ATP hydrolysis, or both (fig. S7C).

Our finding that condensin is an ATP hydrolysis–dependent molecular motor lends support to models invoking SMC protein–mediated loop extrusion as a means for 3D genome organization. An important prediction of the loop extrusion model is that condensin must simultaneously interact with two distal regions of the same chromosome, and at least one (or possibly both) of the interaction sites must translocate away from the other site, allowing for movement of the two contact points relative to one another (Fig. 4A) (12, 14–17). Such "cis" loop geometry is inaccessible in our double-tethered assays because the DNA is held in an extended configuration (Fig. 2A), which likely decouples loop extrusion from translocation. However, a cis loop configuration can be mimicked experimentally by providing a second DNA molecule in trans (Fig. 4B). To test the possible relationship between the observed linear translocation of condensin along the double-tethered DNA and the loop extrusion model, we asked whether condensin could move a second DNA substrate provided in trans relative to the tethered DNA. Indeed, fluorescently labeled (not extended)λ-DNA molecules added in trans to wild-type condensin moved at an apparent velocity of 76 ± 19 bp s−1 (19±5 nm s−1; n =102) (Fig. 4, C and D; movie S2; and data S2) while traveling an average distance of 11 ± 0.9 kb (2.7 ± 0.2 μm; means ± SD; n = 102) (Fig. 4E)— numbers that match well with the measured condensin motor properties reported above. These experiments strongly indicate that translocating condensin complexes were able to interact simultaneously with the tethered DNA and a second DNA. Also, condensin could translocate while bound to both DNA substrates, given that one piece of DNA was observed to move with respect to the other piece of DNA. Thus, we conclude that condensin is capable of moving two DNA substrates relative to one another, fulfilling a key expectation of the loop extrusion model.

Heretofore, a common argument against SMC proteins acting as molecular motors was their low rates of ATP hydrolysis relative to other known nucleic acid motor proteins, which implied that they would not move fast

enough to function as efficient motors on biologically relevant time scales. However, this discrepancy can be readily reconciled if condensin is able to take large steps, which is conceptually possible given its large size of >50 nm. The available data, in fact, suggest a large step size: Comparison of the single complex translocation rate (~60 bp s−1, or ~14.9 nm s−1) with the bulk rate of ATP hydrolysis (k_{cat} = 2.0 s−1 in the presence of linear DNA) indicates that condensin may take steps on the order of ~30 bp per molecule of ATP hydrolyzed. Even larger steps can be inferred if each step is coupled to the hydrolysis of more than one molecule of ATP. These estimates assume that all of the proteins are ATPase-active (one would deduce a smaller step size if a fraction of the protein were inactive) and also assume perfect coupling between ATP hydrolysis and translocation (whereas a more inefficient coupling would necessitate even larger step sizes). The idea that condensin takes very large steps is consistent with the step sizes reported from magnetic tweezer experiments examining DNA compaction induced by *X. laevis*

condensin [80 ± 40 nm; mean ± SD (30)] or *S. cerevisiae* condensin (31). Such large step sizes would seem to rule out models of movement for condensin that resemble those for common DNA motor proteins such as helicases, translocases, or polymerases, which are typically found to move in 1-bp increments (32–35). Higher-resolution measurements may prove informative for further defining the fundamental step size of translocating condensin.

To explain our results, we searched for possible models for condensin motor activity that (i) can explain the relationship between a slow ATP hydrolysis rate relative to the rate of translocation, (ii) can accommodate a very large step size, and (iii) are consistent with the physical dimensions of the SMC complex. Given these criteria, we can think of two theoretical possibilities, both of which use the SMC coiled-coil domains as the means of motility. Condensin might translocate along DNA through reiterative extension and retraction of the long Smc2-Smc4 coiled-coil domains, allowing for movement through a "scrunching" mechanism involving rod- to butterfly-like
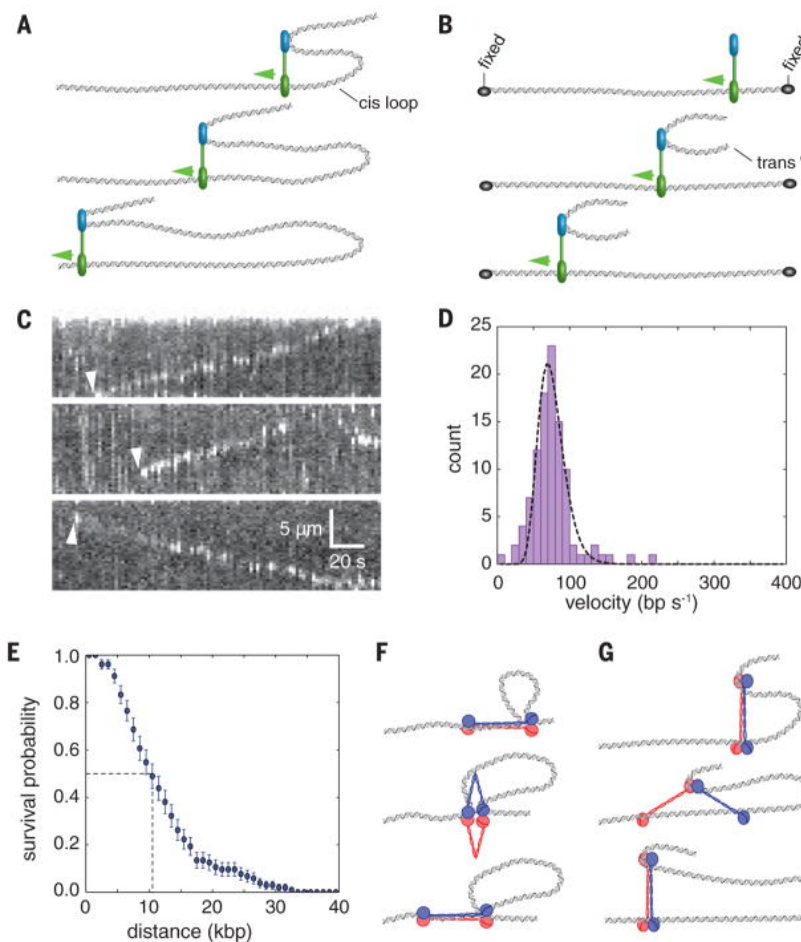

Fig. 4 | Coupling condensin motor activity to DNA loop extrusion. (A) Minimal mechanistic framework necessary for coupling ATP-dependent translocation to the extrusion of a cis DNA loop. In this generic model, a motor domain (green) must move away from another DNA binding domain (blue), and the latter domain can either remain stationary (as depicted) or act as a motor domain and move in the opposite direction (not depicted). **(B)** Detection of cis loop extrusion is not possible when the DNA is held in a fixed configuration, as in the double-tethered curtain configuration that allows for direct detection of condensin motor activity in the absence of condensation (top). The middle and bottom panels show a schematic of an assay to mimic cis DNA loop extrusion by providing a second λ-DNA substrate in trans. **(C)** Examples of kymographs showing translocation of a second λ-DNA substrate (stained with YoYo1) provided in trans in the presence of unlabeled condensin. The presence of the trans DNA substrate is revealed as regions of locally high YoYo1 signal intensity, as highlighted by arrowheads. The regions of higher signal intensity are not detected when the trans DNA is omitted from the reaction. **(D)** Velocity distribution histogram and **(E)** survival probability plot for condensin bound to the trans DNA substrate. The dashed line in (E) highlights the translocation distance corresponding to dissociation of one half of the bound condensin complexes. Error bars represent SD calculated by boot strap analysis. Cartoons of generalized models for condensin motor activity through **(F)** "scrunching" or **(G)** "walking" mechanisms, both of which can be based on ATP hydrolysis–dependent changes in the geometry of the SMC coiled-coil domains.

structural transitions (Fig. 4F); alternatively, condensin may use a myosin- or kinesin-like "walking" mechanism (Fig. 4G). The maximum single step size for each model is defined by the physical dimensions of the SMC coiled-coil domains, corresponding to ≲50 and ≲100 nm for the scrunching and walking mechanisms, respectively (Fig. 4, F and G). Both models are consistent with the range of condensin architectures observed by electron and atomic force microscopy (24, 36). Movements might be powered by ATPase-dependent transitions between different structural states similar to those reported for prokaryotic SMC complexes (21, 37, 38), although it remains to be determined how conformational changes could be translated into the directed movement depicted in our models. Further refinement of the translocation mechanism will depend on fully defining the structural transitions that take place during the ATP hydrolysis cycle and establishing a better understanding of whether (and if so, how) different domains in the condensin complex engage DNA.

Recent Hi-C studies have shown that condensin-dependent DNA juxtaposition occurs at an apparent rate of ~900 bp s−1 in *Bacillus subtilis* (19). This rate is ~15 times as fast as the rates that we observed for single *S. cerevisiae* condensin complexes. However, the apparent rate of in vivo DNA juxtaposition may reflect the cumulative action of multiple condensin complexes functioning in concert. Assuming that there are ~30 SMC complexes per replication origin, and that the mechanism of DNA juxtaposition allows for a linear relationship between the number of SMC complexes present and the rate of DNA juxtaposition, then each *B. subtilis* condensin might be expected to translocate along DNA at a rate of ~30 bp s−1. But these comparisons should be made with extreme caution, because at present it is unclear whether the biophysical properties of the molecular machinery of the prokaryotic system are similar to those of the eukaryotic counterpart, and a recent single-molecule analysis of the *B. subtilis* SMC complex on flow-stretched DNA did not find evidence for translocation on DNA (39). The finding that *S. cerevisiae* condensin is a mechanochemical motor capable of translocating along DNA has important implications for understanding fundamental mechanisms of chromosome organization across all domains of life. We propose that the ATP hydrolysis–dependent motor activity of condensin may be intimately linked to its role in promoting chromosome condensation, suggesting that condensin, and perhaps other SMC proteins, may provide the driving forces necessary to support 3D chromosome organization and compaction through a loop extrusion mechanism. Our findings raise the questions of whether other types of SMC complexes also exhibit intrinsic motor activity and what molecular or regulatory features distinguish SMC motor proteins from those SMC complexes that seemingly lack motor activity.

Author contributions: T.T. designed and conducted single-molecule experiments and data analysis. S.B. purified condensin complexes and conducted bulk biochemical measurements and electron microscopy analysis. J.M.E. designed and implemented single-

molecule experiments. All authors discussed the experimental findings and cowrote the manuscript.

References and Notes

1. Hirano T. Cell. 2016;164:847–857.

2. Uhlmann F. Nat Rev Mol Cell Biol. 2016;17:399–412.

3. Huang CE, Milutinovich M, Koshland D. Philos Trans R Soc Lond B Biol Sci. 2005;360:537–542.

4. Nasmyth K, Haering CH. Annu Rev Genet. 2009;43:525–558.

5. Haering CH, Gruber S. Cell. 2016;164:326–326.e1.

6. Hauk G, Berger JM. Curr Opin Struct Biol. 2016;36:85–96.

7. Guacci V, et al. Cold Spring Harb Symp Quant Biol. 1993;58:677–685.

8. Hirano T, Mitchison TJ, Swedlow JR. Curr Opin Cell Biol. 1995;7:329–336.

9. Peterson CL. Cell. 1994;79:389–392.

10. Niki H, et al. EMBO J. 1992;11:5101–5109.

11. Dekker J, Mirny L. Cell. 2016;164:1110–1121.

12. Nasmyth K. Annu Rev Genet. 2001;35:673–745.

13. Riggs AD. Philos Trans R Soc Lond B Biol Sci. 1990;326:285–297.

14. Alipour E, Marko JF. Nucleic Acids Res. 2012;40:11202–11212.

15. Goloborodko A, Imakaev MV, Marko JF, Mirny L. eLife. 2016;5:e14864.

16. Goloborodko A, Marko JF, Mirny LA. Biophys J. 2016;110:2162–2168.

17. Fudenberg G, et al. Cell Rep. 2016;15:2038–2049.

18. Naumova N, et al. Science. 2013;342:948–953.

19. Wang X, Brandão HB, Le TB, Laub MT, Rudner DZ. Science. 2017;355:524–527.

20. Badrinarayanan A, Reyes-Lamothe R, Uphoff S, Leake MC, Sherratt DJ. Science. 2012;338:528–531.

21. Minnen A, et al. Cell Rep. 2016;14:2003–2016.

22. Cheng TM, et al. eLife. 2015;4:e05565.

23. Piazza I, et al. Nat Struct Mol Biol. 2014;21:560–568.

24. Anderson DE, Losada A, Erickson HP, Hirano T. J Cell Biol. 2002;156:419–424.

25. Kimura K, Hirano T. Proc Natl Acad Sci USA. 2000;97:11972–11977.

26. Greene EC, Wind S, Fazio T, Gorman J, Visnapuu ML. Methods Enzymol. 2010;472:293–315.

27. Stigler J, Çamdere GO, Koshland DE, Greene EC. Cell Rep. 2016;15:988–998.

28. Davidson IF, et al. EMBO J. 2016;35:2671–2685.

29. Qian H, Sheetz MP, Elson EL. Biophys J. 1991;60:910–921.

30. Strick TR, Kawaguchi T, Hirano T. Curr Biol. 2004;14:874–880.

31. Eeftens JM, Bisht S, Kerssemakers J, Haering CH, Dekker C. BioRxiv 149138 [Preprint] 2017 Jun 15; https://doi.org/10.1101/149138.

32. Pyle AM. Annu Rev Biophys. 2008;37:317–336.

33. Singleton MR, Dillingham MS, Wigley DB. Annu Rev Biochem. 2007;76:23–50.

34. Yang W. Annu Rev Biophys. 2010;39:367–385.

35. Seidel R, Bloom JG, Dekker C, Szczelkun MD. EMBO J. 2008;27:1388–1398.

36. Eeftens JM, et al. Cell Rep. 2016;14:1813–1818.

37. Soh YM, et al. Mol Cell. 2015;57:290–303.

38. Bürmann F, et al. Mol Cell. 2017;65:861–872.e9.

39. Kim H, Loparo JJ. Nat Commun. 2016;7:10200.

Materials and Methods

Condensin holocomplex overexpression and purification. The five subunits of the condensin complex were co-overexpressed in *Saccharomyces cerevisiae* from galactose-inducible promoters on 2μ high-copy plasmids (*URA3 leu2-d pGAL7-SMC4(wild-type or Q302L)-StrepII₃ pGAL10-SMC2(wild-type or Q147L) pGAL1-BRN1-HA₃-His₁₂* and *TRP1 leu2-d pGAL10-YCS4 pGAL1-YCG1*; yeast strains C4491 and C4724) as described (*40*), with the following modifications. Cultures were grown at 30°C in –URA–TRP dropout media containing 2% raffinose to OD_{600} of 1. Expression was induced with 2% galactose for 8 hours. Since expression of the Q-loop mutant complex affected the growth rate of the cultures, cells were initially grown at 30°C –URA–TRP dropout media containing glucose to OD_{600} of 1, transferred to media containing 2% raffinose for one hour and then induced by addition of galactose to 2%.

Cells were harvested by centrifugation, re-suspended in buffer A (50 mM TRIS-HCl pH 7.5, 200 mM NaCl, 5% (v/v) glycerol, 5 mM β-mercaptoethanol, and 20 mM imidazole) containing 1× cOmplete EDTA-free protease-inhibitor mix (Roche) and lysed in a FreezerMill (Spex). The lysate was cleared by two rounds of 20 min centrifugation at 45,000 ×g at 4°C and loaded onto a 5-ml HisTrap column (GE Healthcare) pre-equilibrated with buffer A. The resin was washed with five column volumes buffer A containing 500 mM NaCl; buffer A containing 1 mM ATP, 10 mM KCl and 1 mM $MgCl_2$; and then buffer A containing 40 mM imidazole to remove non-specifically bound proteins. Protein was eluted in buffer A containing 200 mM imidazole and transferred to buffer B (50 mM TRIS-HCl pH 7.5, 200 mM NaCl, 5% (v/v) glycerol, 1 mM DTT) using a desalting column. After addition of EDTA to 1 mM, PMSF to 0.2 mM and Tween20 to 0.01%, the protein was incubated overnight with 2 ml (bed volume) of pre-equilibrated Strep-Tactin high-capacity Superflow resin (IBA).

The Strep-Tactin resin was packed into a column and washed with 15 resin volumes buffer B by gravity flow. Protein was eluted with buffer B containing 5 mM desthiobiotin. The eluate was concentrated by ultrafiltration and loaded onto a Superose 6 size exclusion chromatography column (GE Healthcare) pre-equilibrated in buffer B containing 1 mM $MgCl_2$. Peak fractions were pooled and concentrated to 4 μM by ultrafiltration. Purified proteins were analyzed by SDS PAGE (NuPAGE 4-12% Bis-Tris protein gels, ThermoFisher Scientific) and protein bands were identified by in-gel digestion and mass spectrometric analysis.

Nick ligation assays. Nick ligation assays were performed as described earlier (*41*) with the following modifications. A 6.4-kb plasmid containing a single *BbvCI* nicking site was used as a substrate and relaxed by incubation with Nb.BbvCI (NEB). The nicking enzyme was heat-inactivated once the reaction was complete (as confirmed by agarose gel electrophoresis). For assessing supercoiling, reactions were set up in a volume of 20 μl containing 1 nM nicked plasmid DNA and varying amounts of condensin (7.8–500 nM) in 50 mM TRIS-HCl pH 7.5, 100 mM NaCl, 2.5% (v/v) glycerol, 10 mM $MgCl_2$, 1 mM ATP, and 10 mM DTT. Reactions were incubated at room temperature for 30 min before addition of 0.2 μl T4 ligase (5 Weiss U/μl, ThermoFisher Scientific) and fresh 1 mM ATP, followed by an additional 30 min incubation at room temperature to allow the ligation reaction to complete. Reactions were quenched by the addition of 60 μl stop

buffer (50 mM TRIS-HCl pH 7.5, 10 mM EDTA, 1% SDS, 100 μg/ml proteinase K) and incubation at 37°C for 30 min. DNA was purified by phenol-chloroform extraction and ethanol precipitation. The DNA pellet was re-suspended in TE buffer and topoisomers were resolved at 4 V/cm for 9 h on a 0.7% TAE agarose gel containing 0.2 μg/ml chloroquine. The gel running buffer was also supplemented with chloroquine at the same concentration. Gels were stained with ethidium bromide and scanned on a Typhoon FLA 9500 (GE Healthcare).

Pt/C rotary shadowing electron microscopy. Samples for platinum/carbon (Pt/C) shadowing were prepared following the glycerol spray method (*42*). Condensin samples were diluted to a concentration of 0.05 μM in freshly prepared 200 mM NH_4HCO_3 pH 7.5, 30% (v/v) glycerol and 1 mM DTT, immediately sprayed onto freshly cleaved mica and dried under vacuum. Pt/C was shadowed at an angle of 7° followed by deposition of a stabilizing layer of carbon. The Pt/C layers were then floated off and placed onto 100 mesh copper grids. The grids were dried and imaged on a Morgagni TEM (FEI).

Electrophoretic mobility assay. 6-carboxyfluorescein (6-FAM) labelled 45 bp dsDNA was prepared by annealing two complementary HPLC-purified DNA oligonucleotides (IDT, 5'-6-FAM-CCA GCT CCA ATT CGC CCT ATA GTG AGT CGT ATT ACA ATT CAC TGG-3'; 5'- CCA GTG AAT TGT AAT ACG ACT CAC TAT AGG GCG AAT TGG AGC TGG-3') in annealing buffer (10 mM TRIS-HCl pH 7.5, 50 mM NaCl, 1 mM EDTA) at a concentration of 10 μM in a temperature gradient of 0.1°C/s from 95°C to 4°C. 10 μl reactions were prepared with 100 nM 6-FAM-dsDNA and protein concentrations ranging from 50 to 800 nM in reaction buffer (40 mM TRIS–HCl pH 7.5, 125 mM NaCl, 5 mM $MgCl_2$, 10 % glycerol, 1 mM DTT). After 10 min incubation at room temperature (~25°C), free DNA and DNA–protein complexes were resolved by electrophoresis for 10 h at 2 V/cm on 0.8% (w/v) TAE-agarose gels at 4°C. 6-FAM labelled DNA was detected on a Typhoon FLA 9500 scanner (GE Healthcare) with excitation at 473 nm and detection using a 510-nm long pass filter.

Native gel electrophoresis. Protein samples (100 nM) were incubated with 1× and 2× molar ratio of anti-HA Qdots for 10 min at room temperature and the loaded onto a composite agarose-acrylamide gel (0.5% agarose and 2% acrylamide) (*43*). Electrophoresis was performed in TBE buffer at 30V for 10 h at 4°C. The gels were analyzed by silver staining.

ATP hydrolysis assays. ATPase reactions were set up in a volume of 5 μl containing 0.1 μM or 0.5 μM condensin and the indicated concentrations of DNA in 40 mM TRIS-HCl pH 7.5, 125 mM NaCl, 5 mM $MgCl_2$, 0.5 mg/ml BSA and 1 mM DTT. 6.4-kb plasmid DNA had been linearized by *NheI* restriction digest and purified by phenol-chloroform extraction and ethanol precipitation. Reactions were initiated by the addition of ATP at the indicated concentrations (containing 6.7 nM [α-^{32}P]ATP) and incubated at room temperature. At consecutive time intervals, 1 μl of the reaction mix was spotted onto PEI cellulose F TLC plates (Merck). TLC plates were developed in 0.5 M LiCl and 1 M formic acid, exposed to imaging plates and analyzed on a Typhoon FLA 9500 scanner (GE Healthcare). ATP hydrolysis rates were calculated from the change of

ATP/ADP ratios between time points in the linear range of the reaction. Non-linear regression analysis (GraphPad Prism 7.0) was used to estimate the Michaelis-Menten parameters.

Single molecule assays. Double-tethered DNA curtains were prepared as described previously (*26, 27*). Unless otherwise stated, all single molecule measurements were performed in condensin buffer (40 mM TRIS-HCl pH 7.5, 125 mM NaCl, 10 mM MgCl₂, 1 mM DTT, 0.5 mg/mL BSA, and 4 mM ATP) and all assays were conducted at room temperature (~25°C). Quantum dots were labeled with anti-HA antibodies as per the manufacturer's instructions using a SiteClick™ Qdot® 705 Antibody Labeling Kit (ThermoFisher, Cat No. S10454). Purified condensin (1 µl of 1 µM stock) was labeled by mixing with 2 µl anti-HA quantum dots (1 µM) in 7 µl of condensin buffer and incubated on ice for 10 minutes. The labeling reactions were diluted to 100 µl with condensin buffer and then injected into the sample chambers at a flow rate 0.1 ml/min. Flow was then terminated, and the samples were incubated for an additional 20 minutes. Samples were visualized with a custom modified inverted Nikon microscope equipped with a Nikon 60× CFI Plan Apo VC water immersion objective, as described (*26, 27*). Image acquisition was initiated immediately before injecting condensin and continued throughout the 20-minute incubation. All images were acquired with an iXon EMCCD camera (Andor) at a 1 Hz frame acquisition rate. In the absence of nucleotide co-factor, condensin adhered non-specifically to the surfaces of the sample chambers, so all single molecule measurements contained either ATP or ATPγS, as specified.

Particle tracking. The positions ($z(t)$) of each condensin complex were tracked using an in-house Python script. In this script, the intensity profile along DNA was fit with a one-dimensional Gaussian function, taking the mean of the Gaussian fits as the position ($z(t)$) in sub-pixel resolution (*44*). The total length of the λ-DNA substrate used in these experiments is 48,502 base pairs, or 16.49 µm. The DNA is extended to a mean length of ~12 µm in the double-tethered DNA curtains, corresponding to ~72% mean extension, and spans a distance of 48 pixels at 60× magnification. Were indicated, the measured length pixels was converted to base pairs by assuming that each pixel contains 1,010 base pairs of DNA, corresponding to a conversion factor of 4.04 base pairs per nanometer. All particle tracking data are measured in nanometers, and then converted to base pairs for comparison, and both sets of distances are reported. The mean square displacement (MSD) of each trajectory was calculated as $MSD(\Delta t) = \langle z(t + \Delta t)\text{-}z(t)\rangle$.

Translocation of each condensin complex showed a characteristic linear relationship between time and position (Fig. 3A). Thus, data points were fitted with a linear function to calculate slope, which corresponds to the translocation velocity. The resulting translocation velocity data were plotted as histograms, as shown in Fig. 3E, Fig. 4D, and Data S1 and S2, which were well described by log-normal distributions. The functional form of the fits is:

$$f(x) = \frac{A\exp\left[-\frac{1}{2}\left(\frac{\log(x)\text{-}\mu}{\sigma}\right)^2\right]}{\sqrt{2\pi}\sigma x},$$

4

where A is amplitude, $e^{\mu + \frac{\sigma^2}{2}}$ is mean, and $e^{2\mu + \sigma^2}(e^{\sigma^2} - 1)$ is variance. Also, we calculated the reduced chi square values represented by:

$$\chi^2 = \frac{1}{\nu} \sum_i \frac{(n_i - n_{expected,i})^2}{n_i},$$

where n_i is the number of data in i-th bin from the experiments, $n_{expected,i}$ is that from the fitting function. ν is represented by:

$$\nu = n_{all} - p - 1,$$

where n_{all} is the number of all the observations, and p is the number parameters in the fitting function ($p = 3$ in the current work). The goodness of fit for the log-normal distributions was determined by calculating χ^2 values, which were 0.09 and 0.20 for Fig. 3E and Fig. 4D, respectively.

The translocation start (t_s) and end (t_e) times were manually obtained by visual inspection of the data, where the starting time was taken after the brief ~13 s pausing time at the start of the linear trace. A small fraction (6%) of the condensin trajectories displayed a sudden change in direction, and in these instances the translocation end time (t_e) was specified as the time when the molecules changed direction. The distance of translocation was defined as $|z(t_e) - z(t_s)|$, and these values were used to calculate the survival probability plot (*i.e.* processivity) presented in Fig. 3F. The reported processivity values reflect the translocation distance at which one half of the condensin complexes dissociate from the DNA based upon the survival probability plots.

Single molecule trans loop assays. Assays were conducted using double-tethered DNA curtains, as described above. A 100 µL reaction mix was prepared in condensin buffer containing 1 nM condensin, 18 pM free λ-DNA (untagged), and 20 nM YoYo1 (ThermoFisher, Cat. No. Y3601). This reaction mix was then injected at a flow rate of 0.1 ml min⁻¹ into a sample chamber that already contained double-tethered λ-DNA molecules. Note that the tethered λ-DNA was labeled at one end with biotin and at the other end with digoxigenin, as previously described (*26, 27*), whereas the free λ-DNA was not labeled. Buffer flow was then terminated, and the reactions were incubated for an additional 20 minutes at room temperature while capturing 100-millisecond images at 0.2 Hz frame acquisition rate. The laser was shuttered between each 100-millisecond exposure to minimize YoYo1-induced photo-damage. The resulting data were analyzed by particle tracking as describe above.
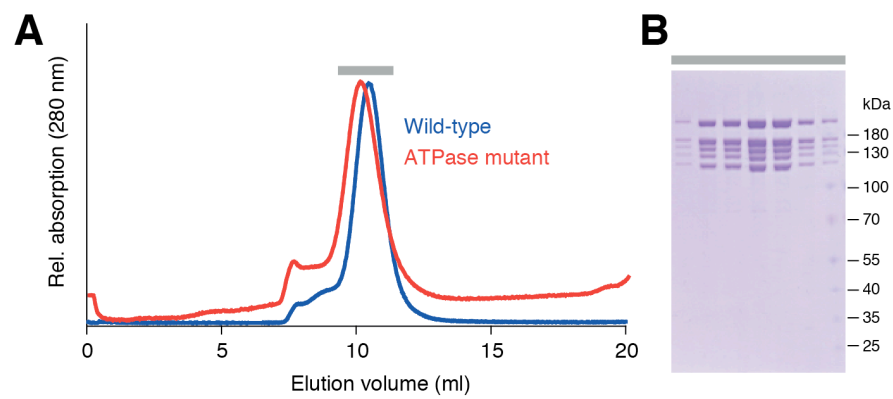
Fig. S1. Purification of budding yeast condensin holocomplexes. (A) Size exclusion chromatograms of wild-type and ATPase-deficient Smc2(Q147L)–Smc4(Q302L) condensin complexes. (**B**) Analysis of peak fractions (grey bar) of the wild-type condensin purification by SDS PAGE and Coomassie staining.
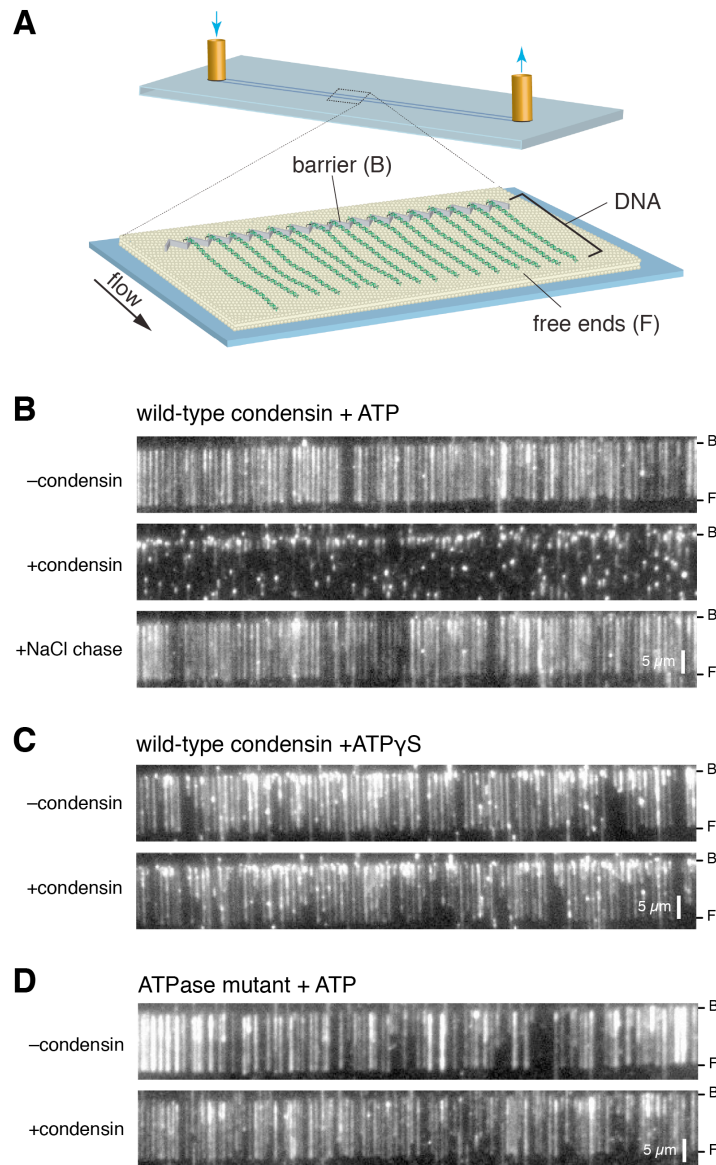
Fig. S2. Condensin can reversibly compact single-tethered DNA curtains. (**A**) Schematic of the single-tethered DNA curtain assay used to test for DNA compaction by unlabeled condensin. (**B**) Still images showing the YoYo1-stained DNA before addition of wild-type condensin, after a 20-minute incubation with 10 nM condensin and 4 mM ATP, and still images after chasing the reactions with 500 mM NaCl. Note that the integrated signal intensity of the extended and compacted DNA molecules should not be compared to one another due the change in the location of the DNA with respect to the penetration depth of the evanescent field. (**C**) Still images showing the YoYo1-stained DNA before addition of wild-type condensin, after a 20-minute incubation with 10 nM condensin and 4 mM ATPγS. (**D**) Still images showing the YoYo1-stained DNA before addition of ATPase deficient condensin, after a 20-minute incubation (in the absence of buffer flow) with 10 nM ATPase-deficient condensin mutant and 4 mM ATP.
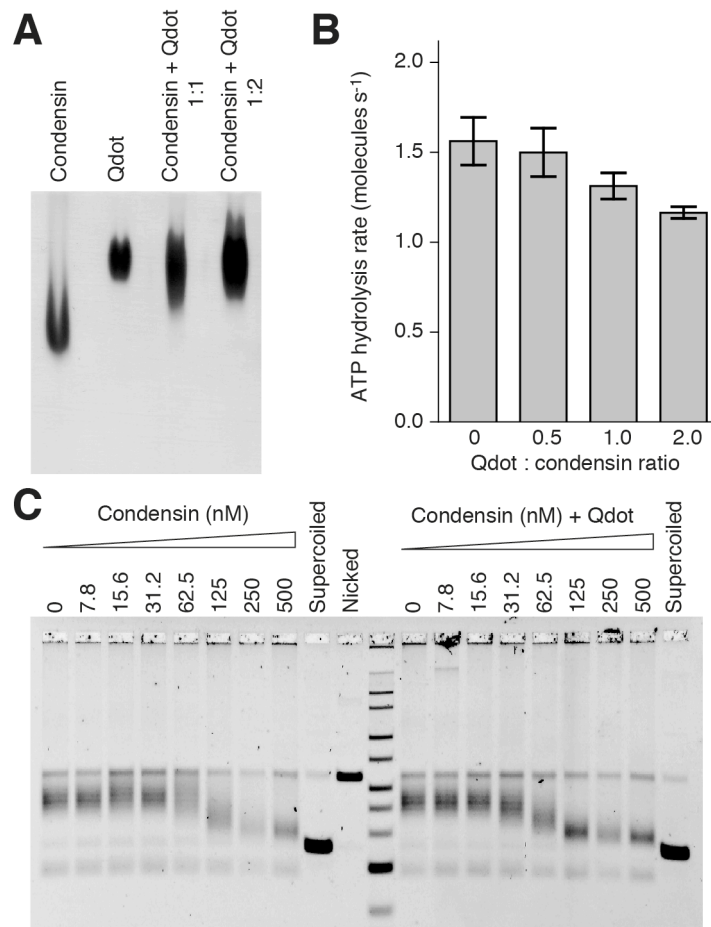
Fig. S3. Condensin labeling with quantum dots. (A) Native composite agarose-acrylamide gel electrophoresis of wild-type condensin complexes upon addition of Qdots coupled to antibodies directed against the HA_3 epitope tag at the C terminus of the Brn1 kleisin condensin subunit. **(B)** Effect of increasing ratios of anti-HA Qdot on the ATPase hydrolysis rate by wild-type condensin complexes (0.1 µM) in the presence of 6.4-kb linear DNA (240 nM) at saturated ATP concentrations (5 mM). **(C)** Nick ligation assay of a 6.4-kb circular DNA (1 nM) with wild-type condensin complexes alone and in the presence of an equimolar amount of anti-HA Qdot.
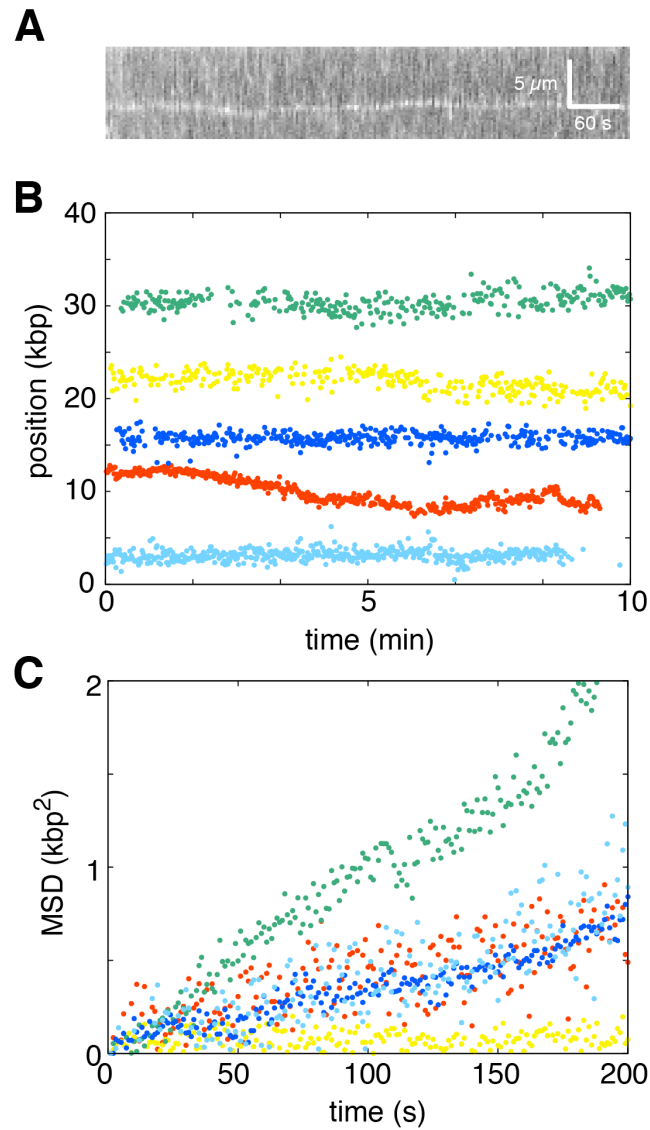
Fig. S4. Condensin exhibits no motor activity in reactions with ATPγS. (A) Kymograph showing condensin bound to DNA in the presence of 4 mM ATPγS. **(B)** Examples of particle tracking data, and **(C)** MSD plots for data collected with wild-type condensin in reactions with 4 mM ATPγS.
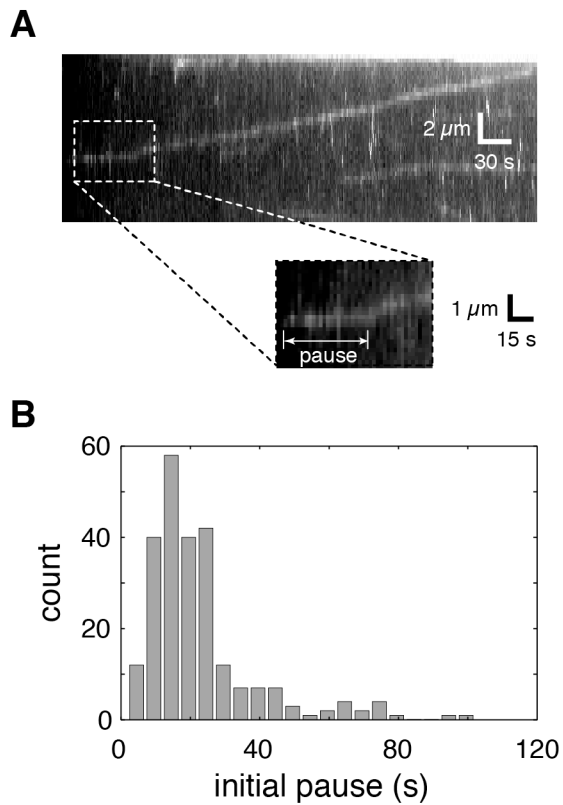
A

2 μm

30 s

1 μm

15 s

pause

B

Fig. S5. Condensin pauses prior to initiating translocation. (**A**) Kymograph highlighting the initial pause (τ_{pause}) prior to the initiation of translocation (also see Fig. 2C). (**B**) Histogram showing the distribution of initial pause times prior to initiating translocation for reactions containing 4 mM ATP.
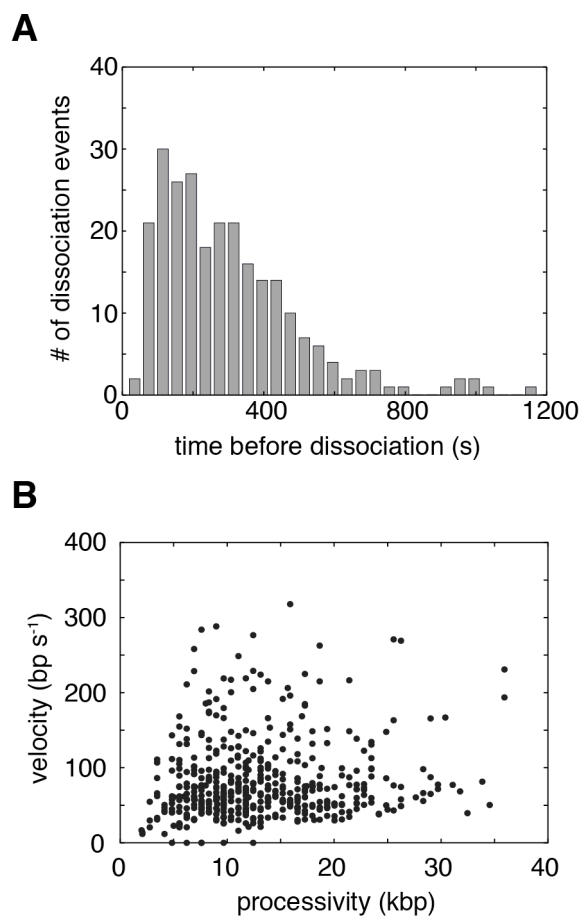
Fig. S6. Condensin's DNA-binding properties. (**A**) Distribution of binding lifetimes for translocating condensin complexes. (**B**) Scatter plot showing that there is no apparent correlation between condensin translocation velocity and processivity. All data shown in this figure reflect results from experiments conducted in the presence of 4 mM ATP.
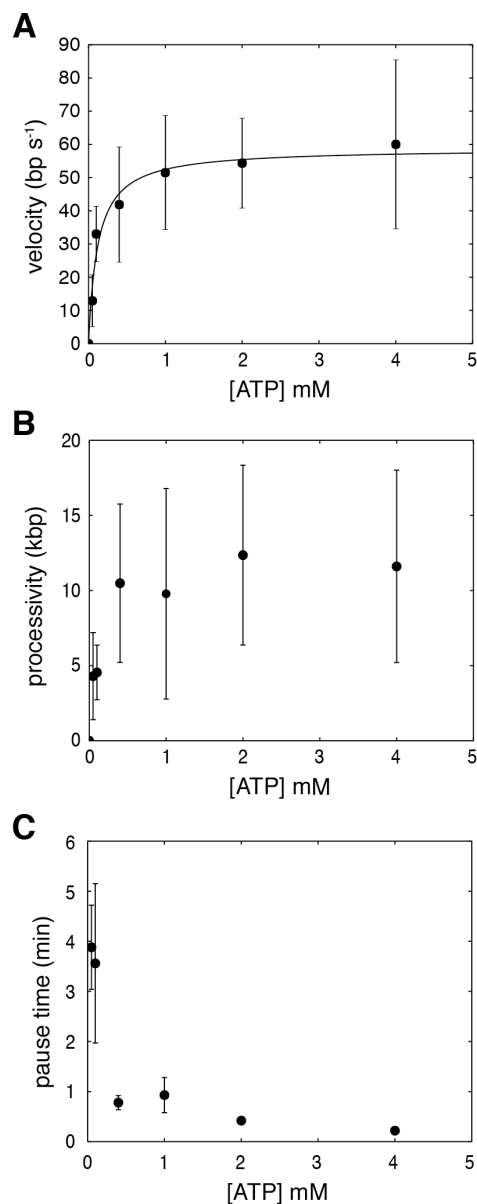
Fig. S7. ATP concentration dependence of condensin translocation characteristics.
(**A**) Condensin translocation velocity versus ATP concentration for data collected at room temperature (~25°C). The data are fit to the Michaelis-Menton equation to extract the kinetic parameters K_m and v_{max}. (**B**) Condensin processivity at different ATP concentrations, as indicated. (**C**) Initial condensin pause times (τ_{pause}) prior to initiating translocation at different ATP concentrations. For each graph, error bars represent standard deviations calculated by boot strap analysis.

Movie S1. Example of condensin translocation on a double-tethered DNA molecule. This video shows a typical example of a ~48-kb double-tethered DNA molecule (unlabeled) bound by quantum dot-tagged condensin. The red arrowhead demarks the initial location of the fluorescent condensin complex on the DNA, and time is indicated in the upper left corner.

Movie S2. Example of condensin translocation on a double-tethered DNA molecule while moving a second DNA provided in trans. This video shows an example of condensin (unlabeled) translocation along a double-tethered DNA molecule while pulling a second λ-DNA substrate provided in *trans*. The DNA is stained with YoYo1, and the location of the *trans* DNA substrate is revealed as the region of locally high YoYo1 signal intensity. The red arrowhead demarks the initial location of the *trans* DNA, and time is indicated in the upper left corner.

Data S1. Particle tracking data for condensin translocation. This PDF file presents all of the raw data pertaining to Fig. 3E for condensin translocation on double-tethered DNA curtains. Each of the data panels (491 total) contains a raw kymograph displaying the movement on condensin on the DNA, a corresponding graph of the particle tracking data for the kymograph, and a linear fit to the tracking data. The slope of the linear fit, reflecting the average velocity for the condensin shown in the kymograph, is also shown.

Data S2. Particle tracking data for trans DNA movement in the presence of condensin. This PDF file presents all of the raw data pertaining to Fig. 4D for condensin translocation on double-tethered DNA curtains while bound to a second DNA in trans. Each of the data panels (102 total) contains a raw kymograph displaying the movement on condensin on the DNA, a corresponding graph of the particle tracking data for the kymograph, and a linear fit to the tracking data. The slope of the linear fit, reflecting the average velocity for the condensin shown in the kymograph, is also shown.